Title

Centrifuge Model Testing of Liquefaction Mitigation via Microbially Induced Calcite Precipitation

Journal

Journal of Geotechnical and Geoenvironmental Engineering, 145(10)

ISSN

1090-0241

Authors

Darby, Kathleen M
Hernandez, Gabby L
DeJong, Jason T
et al.

Publication Date

2019-10-01

DOI

10.1061/(asce)gt.1943-5606.0002122

Peer reviewed

Centrifuge model testing of liquefaction mitigation via microbially induced calcite precipitation

Kathleen M. Darby, S.M. ASCE (Corresponding author)
Senior Staff Engineer, Geosyntec Consultants, 1111 Broadway, Oakland, CA 94607E-mail: kdarby@geosyntec.com

Gabby L. Hernandez, S.M. ASCE
Water Resources Engineer, Department of Water Resources Division of Safety of Dams , 2200 X Street, Sacramento, CA 95818. E-mail: gabby.hernandez-maldonado@water.ca.gov

Jason T. DeJong, M.ASCE
Professor, Department of Civil and Environmental Engineering, University of California at Davis, Davis, CA 95616. E-mail: jdejong@ucdavis.edu

Ross W. Boulanger, F.ASCE
Professor, Department of Civil and Environmental Engineering, University of California at Davis, Davis, CA 95616. E-mail: rwboulanger@ucdavis.edu

Michael G. Gomez, A.M.ASCE
Assistant Professor, Department of Civil and Environmental Engineering, University of Washington, Seattle, WA 98195. E-mail: mggomez@uw.edu

Daniel W. Wilson, M.ASCE
Assoc. Dir, Center for Geotechnical Modeling, University of California at Davis, Davis, CA 95616. E-mail: dxwilson@ucdavis.edu

Authors' final copy (March 2019) prior to copyediting and publication
in the Journal of Geotechnical and Geoenvironmental Engineering

ABSTRACT

A set of saturated Ottawa sand models were treated with Microbially Induced Calcite Precipitation (MICP) and subjected to repeated shaking events using the 1-m radius centrifuge at the UC Davis Center for Geotechnical Modeling. Centrifuge models were constructed to initial relative densities (D_{R0}) of approximately 38% and treated to light, moderate, and heavy levels of cementation (calcium carbonate contents by mass of approximately 0.8%, 1.4%, and 2.2%, respectively) as indicated by shear wave velocities (light ≈200 m/s, moderate ≈325 m/s, and heavy ≈600 m/s). The cemented centrifuge models are compared to a pair of uncemented saturated Ottawa sand models with initial D_{R0}s of ≈38 and ≈53% and subjected to similar levels of shaking. Cone penetration resistances and shear wave velocities are monitored throughout shaking to investigate (1) the effect of cementation on cone penetration resistance, shear wave velocity, and cyclic resistance to liquefaction triggering and (2) the effect of shaking on cementation degradation. Accelerometers, pore pressure transducers, and a linear potentiometer are used to monitor the effect of cementation on liquefaction triggering and consequences. Cone penetration resistances and shear wave velocities are sensitive to light, moderate, and heavy levels of cementation (increases in penetration resistance from 2 to 5 MPa, 2 to 10 MPa, and 2 to 18 MPa and shear wave velocity from 140 to 200 m/s, 140 to 325 m/s, and 140 to 660 m/s, respectively), and are able to capture the effects of cementation degradation.

INTRODUCTION

Liquefaction of loose saturated sands is a serious concern in seismically active regions due to the detrimental consequences observed after earthquake loading (e.g., bearing failures underneath buildings, uplift of buried tanks, and failure of bridges and embankments). Current ground improvement methods to mitigate liquefaction include dynamic compaction, chemical grouting, and deep soil mixing, amongst others; however, these methods are typically energy intensive and have the potential to negatively impact the environment (Karol 2003, Raymond et al. 2017). Microbially Induced Calcite Precipitation (MICP) is an alternative bio-mediated ground improvement method that utilizes soil microorganisms to induce calcite precipitation within sandy soils. MICP achieves bio-cementation through the addition of calcium ions in treatment solutions and microbial urea hydrolysis wherein urease enzymes hydrolyze supplied urea to produce ammonia and dissolved inorganic carbon (Fujita et al. 2008). Bio-cementation has been shown to improve the engineering properties of sands including: increased initial shear stiffness, peak shear strength, and resistance to liquefaction triggering (DeJong et al. 2006; Whiffin et al. 2007; Montoya et al. 2013; Montoya and DeJong 2015; Zamani and Montoya 2017; Darby et al. 2018; Feng and Montoya 2017; Xiao et al. 2018).

Prior research on MICP treated sands subjected to dynamic loading has shown that bio-cementation has the potential to significantly increase the resistance of liquefaction triggering of granular soils. The strength related benefits of MICP-treatment include: particle bonding (cementation), increased density, and increased angularity which results in stronger dilative tendencies (Montoya and DeJong 2015; Feng and Montoya 2015). Though degradation of cementation during liquefaction triggering is expected to reduce the cementation benefit, the other benefits (increased density and angularity) will remain, though a small portion of the

calcium carbonate ($CaCO_3$) may become free in the pore space. For the $CaCO_3$ content treatment levels applied in the following past studies as well as in this paper, the amount of free $CaCO_3$ would be less than 5% by mass and would likely have an insignificant effect on subsequent liquefaction behaviors. Montoya et al. (2013) conducted a series of centrifuge tests on untreated and MICP-treated models subjected to a sequence of shaking events with generally increasing shaking amplitude. The MICP treated soils exhibited reduced excess pore pressure generation, reduced settlements, and generally greater surface accelerations, when compared to untreated loose models. As the level of cementation increased, a transition in soil behavior from 'soil-like' to 'rock-like' was observed (Montoya et al. 2013). More recently, a pair of untreated and lightly bio-cemented loose saturated Ottawa sand centrifuge models were subjected to multiple shaking events, with results indicating a stronger base acceleration is required to generate an excess pore pressure ratio (r_u) of 0.95 in an MICP treated model when compared to an untreated model (Darby et al. 2019). Zamani and Montoya (2017) conducted cyclic direct simple shear (DSS) tests on untreated and MICP treated silty Nevada Sand (fines content = 15%) specimens subjected to a cyclic stress ratio (CSR) of approximately 0.2 until triggering liquefaction, defined by reaching 3% single-amplitude (SA) shear strain. Results showed that untreated and MICP treated samples required 4 and 91 cycles, respectively, to reach 3% SA strain; the increase in liquefaction resistance was attributed to an increase in density and improved load transfer and undrained shear strength from cementation bonds. Feng and Montoya (2017) performed cyclic triaxial (TX) tests on two identical specimens of loose Ottawa 50-70 sand treated with MICP to shear wave velocities (V_s) of 425 m/s and 676 m/s. The results showed that MICP treated sands with higher cementation levels (as indicated by V_s) require almost one order of magnitude more loading cycles (98 and 963 cycles, respectively) prior to

significant accumulation of strains and excess pore pressure generation. Similarly, in a series of undrained cyclic TX tests, Xiao et al. (2018) showed that MICP treated calcareous sands generate lower excess pore pressure and compressive strains and a significant increase in the number of cycles to trigger liquefaction compared to clean calcareous sands (Xiao et al. 2018).

Currently, measurements of soil calcium carbonate ($CaCO_3$) content, V_s, and cone penetration resistance (q_c) are the primary metrics available for in-situ assessment of MICP cementation level. V_s measurements have the advantage of being non-destructive, can be measured on small laboratory samples, and provide a direct measurement of the small-strain shear stiffness. Furthermore, Feng and Montoya (2017) showed that the behavior of cemented sands subjected to cyclic loading depends on the distribution of $CaCO_3$, which is better captured by V_s than by measuring the average $CaCO_3$ content. Burbank et al. (2013) pushed a miniature cone penetrometer in a 46 cm deep treated box and was able to detect the effects of as little as 2% $CaCO_3$ precipitation at depths greater than 20 cm. At the meter-scale, MICP treated column tests conducted by Gomez et al. (2016, 2018), observed increases in $CaCO_3$ content were consistent with increases in V_s and q_c. These results suggested V_s measurements are more sensitive than q_c to low levels of cementation (near 1% $CaCO_3$ by mass) and that cone penetration measurements require higher levels of cementation (greater than 3% $CaCO_3$ by mass) to definitively detect cementation (Gomez et al. 2016, 2018).

The effect of repeated shaking events on the cyclic strength of saturated, uncemented sands has been examined in a number of prior centrifuge studies (e.g. Sharp et al. 2010, Su et al. 2013, El-Sekelly et al. (2015, 2016, 2017), Darby et al. (2016, 2019), Dobry et al. 2015, Dobry and Abdoun (2017), Okamura et al. 2017, Wang et al. (2018)). Darby et al. (2016, 2019) performed dynamic centrifuge tests conducted on loose and dense, clean, uncemented, saturated

Ottawa sands subjected to repeated shaking events, and demonstrated that the normalized q_c and cyclic resistance ratio (CRR) gradually increased due to past shaking and repeated liquefaction events. The correlation between q_c and CRR from the centrifuge studies was relatively consistent with CPT-based liquefaction triggering correlations from case history data, suggesting that both parameters can account for the variations in relative density and shaking history (Darby et al. 2019). Additional centrifuge studies have observed q_c to be more sensitive to the effects of shaking history than V_s measurements (Dobry and Abdoun 2017). El-Sekelly et al. (2015, 2016) conducted a set of centrifuge tests on saturated silty sand models and observed that although low amplitude repeated shaking significantly increased liquefaction resistance, the increase was not reflected by the increase in V_s (less than 10% increase). An additional study observed that extensive liquefaction resulted in a temporary decrease in liquefaction resistance (El-Sekelly et al. 2016).

In the current study, untreated and MICP treated centrifuge models are subjected to repeated shaking to investigate the effects of MICP on the initial resistance to liquefaction triggering, the degradation of cementation with shaking history, and the ability of q_c and V_s to capture these effects. Three saturated F-65 Ottawa sand models prepared at D_{R0} of approximately 38% are treated to a light, moderate, or heavy level of cementation and then subjected to nine to eleven shaking events with peak base accelerations (PBA) ranging from 0.02 to 0.55 g while at an 80-g centrifugal acceleration. The behavior of the cemented models is evaluated against a pair of uncemented saturated F-65 Ottawa sand models prepared at D_{R0}s of approximately 38% and 53% and subjected to similar shaking sequences as the cemented models, consisting of eleven and sixteen shaking events, respectively. Matching arrays of accelerometers (ACC) and pore pressure transducers (PPT) in all models are used to define

CSRs, shear strains, and excess pore pressure generation. A mini-cone penetrometer was pushed at select times during each test to evaluate the ability of the cone to capture the effects of initial cementation and cementation degradation. Similarly, horizontal V_s measurements were obtained prior to each cone push and shaking event using two arrays of bender element (BE) pairs placed at matching depths. Cone penetration resistances at mid-depth increased from 2 to 5 MPa, 2 to 10 MPa, and 2 to 18 MPa in lightly, moderately, and heavily cemented models. V_s at mid-depth increased from 140 to 200 m/s, 140 to 325 m/s, and 140 to 660 m/s in lightly, moderately, and heavily cemented models at 80 g. Cone penetration resistances and V_s after initial liquefaction decreased significantly in moderately and heavily cemented models, decreased slightly in lightly cemented models, and increased slightly in uncemented models. Irregular CSR time series at different depths are derived from the recorded accelerations, converted to equivalent uniform time series (as described later) and then paired with normalized cone penetration resistances ($q_{cN} = q_c/P_A$ where P_A = atmospheric pressure) and V_s values for the same depth intervals. Cemented models required stronger PBAs and CSRs to trigger liquefaction compared to the uncemented model prepared to a similar relative density, even after initial liquefaction. CSR-q_{cN} and CSR-V_s pairs are compared to existing CPT q_c and V_s based liquefaction triggering correlations for clean sands. Compiled CSR, q_c, V_s, and dynamic responses are available in tables S-1 through S-5 of the electronic supplement.

CENTRIFUGE MODEL AND TESTING SEQUENCE

Model construction and instrumentation

A set of centrifuge models consisting of Ottawa F-65 sand placed at $D_{R0} \approx 38\%$ were constructed to the dimensions provided in Figure 1 in a flexible shear beam container at the UC Davis Center

for Geotechnical Modeling. Models were constructed in a series of five lifts with thicknesses of 20 mm (lifts one through four) and 30 mm (lift five) using the method of dry pluviation to a final thickness of 110 mm. The Ottawa sand layer was underlain by a hand compacted 30 mm saturation layer consisting of pea gravel and O-30 Monterey sand to assist in cementing the sand layer. Constructed models were saturated under vacuum with de-aired deionized (DI) water.

Models were instrumented with ACCs, PPTs, and BEs at the locations indicated in Figure 1. Twelve BEs were placed as pairs at three depths in two vertical array locations (A-1 and A-2), with an average tip-to-tip spacing of 73 mm. A 50 mm stroke LP was attached to the container prior to shaking events to measure surface settlement. Additionally, ACCs were attached to the exterior of the container to measure achieved horizontal base accelerations.

A pair of uncemented models were prepared at D_{R0}s of 38% and 53% to provide baseline behavior against which the MICP cemented models can be compared. Uncemented models were constructed and instrumented using the same procedures as previously described for the cemented models. Following construction, uncemented models were saturated under vacuum with a solution of methycellulose and DI water prepared to a viscosity of approximately $5x10^{-5}$ m^2/s.

MICP treatment

After initial saturation, MICP treated models (all prepared to $D_{R0} \approx 38\%$) were inoculated and treated at 1-g. A highly active ureolytic bacterium, *Sporosarcina pasteurii* (*S. pasteurii*) and a $CaCl_2$-urea solution was used to facilitate $CaCO_3$ precipitation. *S. pasteurii* was introduced to the model in an inoculation solution consisting of $4x10^7$ cells/ml in an isotonic 154 mM sodium chloride solution. Inoculation was performed in two stages. In the first stage, 10 L (approximately two pore volumes) of inoculation solution was injected to the model via six ports

in the base of the container at a rate of approximately 0.15 L/min and was collected at the surface via a drainage port in the top shear ring. In the second stage, 20 L of inoculation solution was percolated from the surface downward while pumping solution out the base ports at a rate of approximately 0.35 L/min. Prior to inoculation, a light overburden (0.1 kPa) was applied to the model. At the end of inoculation, approximately 4 kPa of additional overburden was added to the model's surface and flow was halted for approximately 6 hours to allow *S. pasteurii* sufficient time to attach to soil particles.

After inoculation, models received multiple rounds of cementation treatments to achieve light, moderate, or heavy levels of cementation, as indicated by V_s measurements. Each cementation treatment consisted of two stages as follows. The first stage consisted of a 5 L flush solution containing urea (350 mM), yeast extract (0.2 g/L), and sodium acetate (4.25 mM) to remove excess carbonate ions, as per Gomez et al. (2016). The second stage consisted of a 10 L treatment solution, containing the same constituents and concentrations as the flush solution, with the addition of $CaCl_2$ (250 mM). Both flush and treatment solutions were pumped through the base ports at a rate of 0.35 L/min. Cementation treatments were separated by approximately 12 hours to allow precipitation reactions to reach completion. V_s was measured at 1-g before each treatment and 12 hours after each treatment. Figure 2 a-c presents the evolution of V_s with treatment for the lightly, moderately, and heavily cemented models, respectively. The uppermost BE pair in A-1 did not work in all tests and is therefore not shown. As indicated in Figure 2, all models start at an initial V_s of $\approx$ 80 m/s and increase approximately linearly with each treatment. It is worth noting that the rate of increase varies between models, which may reflect differences in bacterial cell distributions and activities. The lightly, moderately, and heavily cemented models received two, three, and four treatments, respectively, and achieved final 1-g V_ss of

approximately 220, 350, and 670 m/s, respectively. $CaCO_3$ content measurements were obtained at the end of each model test at the locations indicated in Figure 1. $CaCO_3$ contents were approximately 0.8%, 1.4%, and 2.2% in the lightly, moderately, and heavily cemented models, respectively. The distribution of $CaCO_3$ in each of the cemented models is provided in Table 1. As indicated in Table 1, while there is some variation in the distribution of $CaCO_3$ in each model, the overall distribution is reasonably uniform.

After reaching the target V_s level, ≈ 40 L of a deaired solution of methycellulose and DI water prepared to a viscosity of ≈ 5 x10^{-5} m^2/s was pumped through each cemented model from the base ports at a rate of 0.35 L/min. Previous studies (e.g., Darby et al. 2018) had not increased the pore fluid viscosity post treatment, and they observed significant drainage effects during shaking. Based on those observations, this study used an increased pore fluid viscosity to better match dynamic scaling laws at elevated g-level and minimize partial drainage during cyclic loading while ensuring the model was constructible (Stewart et al. 1998). V_s measurements before and after indicated minimal changes due to the viscous fluid inundation.

Centrifuge model testing

All models were spun to a centrifugal acceleration of 80-g and subjected to nine to sixteen shaking events with amplitudes of acceleration ranging from 0.02 to 0.55g. For the remainder of this paper, all units are presented in prototype unless otherwise noted. Each shaking event consisted of 15 cycles of a uniform amplitude 1.25 Hz frequency sine wave. Accelerations and pore pressures were monitored during and after each shaking event, and V_s was measured before and after each shaking event. Shaking events were separated by ≈ 10 min (model units) to ensure full dissipation of excess pore pressures, though full dissipation was observed after ≈ 1 min (model units).

A 6 mm diameter cone (model units) was pushed at a rate of 10 mm/s at select times during each centrifuge model test at the locations indicated in Figure 1. Cones were pushed before treatment (cemented models) (cone 0), before any shaking (cone 1), after initial liquefaction triggering (cone 2), and after the last shaking event (cone 3). The pre-treatment cone in cemented models was used to evaluate the effect of cementation and ensure initial D_{R0} compatibility with the initially loose uncemented model.

A second moderately cemented model was constructed to investigate the influence of g-level and repeated spin-up/spin-down (loading-unloading) cycles on cementation integrity, as measured by V_s and q_c. This additional model was subjected to four centrifugal loading-unloading cycles (with no dynamic shaking events), with each cycle starting and ending at 1-g and reaching maximum g-levels of 20-g, 40-g, 60-g, and 80-g, respectively, in 20-g increments. A cone was pushed at the maximum g-level in each loading-unloading cycle at a unique location along the centerline of the model. V_s measurements were obtained prior to each cone push and each time the model was spun to 1-g, 20-g, 40-g, 60-g, and 80-g. V_s was also obtained after the final cone push (cone 4). These measurements were used to investigate the influence of g-level and multiple loading-unloading cycles on q_c and V_s.

The influence of confining stress and number of loading-unloading cycles (without any dynamic shaking events) on shear stiffness is examined against vertical effective stress in Figure 3a. Measurements obtained at each g-level are indicated as circles, with the shading of circle corresponding to the number of times the model has experienced a given stress level, and black arrows indicating the sequence of loading-unloading. Also shown in Figure 3a are results from the uncemented loose model and the lightly, moderately, and heavily cemented models subjected to two loading-unloading cycles from 1-g to 80-g. The shear stiffness behavior of models

subjected to the same maximum stress level in fewer loading-unloading cycles provides insight on the relative importance of stress level and number of loading-unloading cycles on cementation integrity. The cemented models subjected to two loading-unloading cycles indicate relatively little influence of effective stress on shear stiffness, with the amount of influence dependent on cementation level. These observations are consistent with those by Montoya et al. (2013), though the maximum g-level in their experiments was 50-g compared to 80-g in this study. The moderately cemented model subjected to multiple loading-unloading cycles indicates little dependence of shear stiffness on effective stress during the first three loading-unloading cycles. After the third loading-unloading cycle, the shear stiffness at 1-g (48 MPa) is significantly reduced from the initial value (242 MPa) and continues to decrease as the model is subjected to higher effective stresses. This behavior suggests a maximum number of loading-unloading cycles before significant stiffness degradation occurs. To evaluate whether significant stiffness degradation had occurred during each model test, V_s measurements were obtained each time a model was spun-down to 1-g and back up to 80-g and compared to the initial values.

The effect of g-level on the average q_c at mid-depth (± 2.5 dia.) in the additional moderately cemented model for the first loading to each g-level (and without any shaking events) is shown in Figure 3b. Overall, q_c increases from 5.5 MPa at 20-g to 8.7 MPa at 80-g. Unexpectedly, q_c slightly decreases at 40-g to 5.2 MPa. This decrease potentially results from cementation non-uniformity, both laterally and with depth, as the reported q_c values are averages over a 5 cone diameter interval. Mid-depth $CaCO_3$ contents at the 20-g and 40-g cone locations are comparable (1.2 and 1.1%) while at the deeper range of the averaging zone the $CaCO_3$ content at the 20-g cone location is larger than at the 40-g cone location (1.6 and 1.3%).

Progressive changes in V_s throughout the entire testing sequence are shown in Figures 4a-d for the uncemented initially loose and the lightly, moderately, and heavily cemented models, respectively. The shape of the symbol indicates the depth of the BE pair; symbol shading indicates BE array, A-1 or A-2. The background shading indicates whether the measurement was obtained at 1-g (gray) or at an elevated g-level (white). All elevated g-level measurements are obtained at 80-g unless otherwise noted. V_s measurements were obtained before each cone push as well as after inoculation, each treatment and the viscous fluid flush. The timing of V_s measurement relative to each shaking event (S) is indicated along the x-axis. The occasional data gaps in Figures 4c and 4d are due to equipment difficulties in consistently obtaining BE readings at high g-levels, particularly in the more cemented models. The limited V_s readings in moderately cemented model during the initial spin-up to 80-g suggest V_s decreased with increasing g-level; this behavior is unexpected, but given the gaps in the BE readings, additional research is needed to determine if the observed behavior is significant. As mentioned earlier, the reduction in shear stiffness due to loading-unloading cycles can be evaluated by comparing the V_s at 80-g prior to a spin-down to the V_s at 80-g after the spin-down. V_s in the lightly cemented model decreases slightly after the first loading-unloading cycle, but does not significantly decrease after each of the remaining three cycles. V_s in the moderately cemented model decreases after the second loading-unloading cycle, but does not decrease after the third or fourth cycle.

DYNAMIC RESPONSES

Time series of shear stress and shear strain are calculated from filtered acceleration records using the procedures by Kamai and Boulanger (2010) and Brandenberg et al. (2010), respectively.

Accelerations are filtered using a zero phase delay 4th order Butterworth bandpass filter with corner frequencies of 0.01 and 100 Hz. The Kamai and Boulanger (2010) method to calculate shear stresses is a mass weighted procedure assuming accelerations vary linearly between nodes. The Brandenberg et al. (2010) procedure uses the method of weighted residuals to calculate shear strains from double integrated filtered accelerations. CSR time series are computed by normalizing cyclic shear stress time series by initial vertical effective stress ($CSR= \tau/\sigma'_{v0}$).

The shaking sequences for the uncemented and cemented models are shown in the bottom plots of Figure 5. Data for the uncemented models are shown in the left panel, data for the cemented models are shown in the right panel. Shading intensity corresponds to increasing D_{R0} (uncemented models) or cementation level (cemented models). The lightly and moderately cemented models were subjected to progressively increasing PBAs ranging from 0.02g to 0.24g and 0.20g, respectively; the heavily cemented model was subjected to strong shaking events (PBA= 0.45-0.5g) until liquefaction was triggered (defined in this study as achieving an excess pore pressure ratio ($r_u=u_e/\sigma'_v$ where u_e= excess pore pressure) of 0.95), after which the model was subjected to the same shaking sequence as the lightly and moderately cemented models. After triggering the lightly, moderately, and heavily cemented models (at PBA=0.10g, 0.17g, and 0.45g, respectively), each cemented model was subjected to 0.06g PBA, the PBA required to trigger the uncemented initially loose model, to evaluate the effect of liquefaction triggering on cyclic strength. The uncemented initially loose model was subjected to the same shaking amplitude and sequence as the lightly cemented model; the moderately dense model was subjected to repeated shaking events at its triggering PBA until liquefaction was no longer triggered.

Also shown in Figure 5 are q_c, V_s, maximum shear strain (γ_{max}), and r_u at mid-depth for uncemented and cemented models. As mentioned previously, there were two BE pairs at mid-depth in each model. V_s readings are not averaged between the BE pairs at mid-depth. In some cases, (e.g., the lightly cemented model) these pairs gave slightly different readings; in other cases, (e.g., the uncemented models) these pairs gave nearly identical readings. V_s readings were obtained prior to each shaking event as well as after the shaking event triggering initial liquefaction and after the final shaking event. The uncemented initially loose model first liquefied at a PBA of 0.06g and continued to liquefy during the remaining eleven shaking events, generating γ_{max} ranging from 0.2 to 1.7%. V_s remained constant throughout all shaking events while q_c progressively increased, with the majority of the increase occurring during the last six shaking events. The greater increase in q_c between the second and third cone push compared to the increase between the first and second cone push is consistent with the shaking events in the second interval having larger PBAs, generating higher r_u and larger γ_{max}, and the soil correspondingly experiencing a greater amount of densification. The lightly cemented model required a PBA of 0.10g to trigger liquefaction ($r_u > 0.95$) and generated $\gamma_{max} = 1.6\%$; V_s and q_c decreased slightly after triggering and then remained relatively constant during the remainder of the shaking events. The moderately cemented model required a PBA of 0.17g to trigger and generated $\gamma_{max} = 0.6\%$. V_s decreased from 300 to 270 m/s after triggering, and remained relatively constant after the sixth shaking event; q_c decreased from 10 to 4 MPa after triggering, and increased to 6 MPa during the final three shaking events. The heavily cemented model was subjected to three shaking events with PBA ranging from 0.5g to 0.45g, until liquefaction was triggered during the third shaking event, generating $\gamma_{max} = 0.6\%$. During the two strong shaking events prior to triggering V_s progressively decreased to 300 m/s. After triggering, V_s further

decreased to 275 m/s, but remained relatively constant until the final two shaking events, which had PBAs of 0.27g and 0.30g, respectively. The q_c decreased from 18 to 10 MPa after triggering and remained relatively constant during the seven remaining shaking events. During initial triggering, the heavily cemented model generates a r_u much larger than 1.0, suggesting the soil could hold tension. This observation is attributed to the heavily cemented model having cohesion. None of the cemented models triggered when subjected to the PBA required to trigger the uncemented loose model following their initial triggering events. This observation suggests that triggering-induced cementation degradation was not sufficient to return the model to the uncemented condition, which is expected because the precipitated calcite had increased soil density and particle angularity in addition to cementing the soil particles.

Figure 6 compares the dynamic responses for the uncemented initially loose model to the dynamic responses for the lightly, moderately, and heavily cemented models at the PBA required to trigger initial liquefaction in each of the models. Excess pore pressures at the three measured depths are shown in the top plot, followed by the acceleration at the upper ACC (approximately 2.0 m from the surface), CSR at mid-depth, γ at mid-depth, and finally base acceleration in the bottom plot. Surface settlement for each event and initial vertical effective stress at each PPT are provided below each plot stack. Comparison of the dynamic responses in the uncemented and cemented models indicate some interesting behavior. While the uncemented model exhibits de-amplification of the acceleration, the cemented models exhibit amplification of accelerations prior to and during triggering. In the uncemented model, the input PBA of 0.06g is slightly amplified near the surface to a value of 0.07g, before decreasing to $\approx$ 0.02g later in shaking. In the lightly, moderately, and heavily cemented models the input PBAs of 0.10g, 0.17g, and 0.45g are amplified near the surface to values of 0.29g, 0.49g, and 0.56g, respectively. PPTs at all

three depths trigger within approximately 2 s of each other in each cemented model, with the lower PPT generally triggering first. This observation combined with the amplification at 2 m depth may suggest cemented sands experience a reduction in cyclic resistance ratio at higher effective stress, which is consistent with findings by Simatupang and Okamura (2017) based on a series of undrained cyclic triaxial tests on cemented sands with confining stresses ranging from 50 to 200 kPa. However, the effective stresses in this study (approximately 20 to 50 kPa) are lower than those examined by Simatupang and Okamura (2017), and the lack of dense accelerometer arrays limits the ability in this study to reliably track how CSR and pore pressure evolve throughout the model. This limitation complicates the correlation of cyclic resistance ratio with effective stress. Additional studies are needed to evaluate the CRR stress-level dependency for cemented sands, particularly at effective stresses below 50 kPa. Shear strains in the uncemented model are below 0.5%, while the lightly and moderately cemented models reach shear strains of 1.6% and 0.6%, respectively. The shear strains in the heavily cemented model are less reliable due to the strong, high-frequency accelerations (i.e., more sensitive to filtering and processing procedures), but reach a value of 0.6%. Additionally, the pore pressure behavior in the heavily cemented model exhibits large negative dilation spikes not present in the uncemented or the lightly and moderately cemented models.

CONE PENETRATION RESISTANCES

Three cones were pushed in each of the untreated loose and medium dense models. Cones were pushed before any shaking, after shaking event five, and after the last shaking event was completed. The initially loose uncemented model first triggered liquefaction after shaking event 2; the initially moderately dense uncemented model first triggered after shaking event 4.

Penetration resistances for the initially loose and moderately dense uncemented models are shown in Figure 7a and 7b, respectively. In both uncemented models there is minimal change in q_c at mid-depth after four and two liquefaction events, respectively, and a large increase in q_c after the last shaking events (11 and 16, respectively).

Four cones were pushed at select times in each of the lightly, moderately, and heavily cemented models to capture the effects of initial cementation and shaking on q_c. A cone was pushed (1) prior to cementation, (2) at 80g but before any shaking, (3) after first triggering (shaking events five, six, and three , respectively), and (4) after the last shaking event (shaking events 11, 9, and 10, respectively). The cones pushed prior to cementation were also used to ensure consistency with the uncemented initially loose model.

Cone penetration resistances in the uncemented models are compared to q_c in the cemented models in Figure 7. Prior to cementation, the q_c at mid-depth in the lightly, moderately, and heavily cemented models are 2.2, 2.3, and 2.0 MPa, respectively, compared to an initial mid-depth q_c of 2.3 MPa in the uncemented initially loose model. After cementation, the q_c of the lightly, moderately, and heavily cemented model increases to 4.6, 9.9, and 17.8 MPa, respectively. After triggering liquefaction, mid-depth q_c decreases minimally in the lightly cemented model to 3.8 MPa, and significantly in the moderately and heavily cemented models to 4.5 and 9.9 MPa, respectively. At the last shaking event, the mid-depth q_c in the lightly cemented model has slightly increased back near the initial value of 4.5 MPa, the moderately cemented model has increased to 6.3 MPa, and the heavily cemented model has decreased slightly to 9.6 MPa.

The behavior of q_c in the uncemented and cemented models during multiple shaking events suggests the interaction of three hypothesized mechanisms: densification of soil skeleton,

damage to cemented bonds, and reduction in initial void ratio by addition of precipitate. The first mechanism, densification, is exhibited by the behavior of the uncemented models, where q_c progressively increases with multiple shaking events. This progressive increase has been observed in previous centrifuge tests of uncemented models (e.g. Darby et al. 2019). Densification is also observed between liquefaction triggering and the end of shaking in the moderately cemented model, and to a lesser degree in the lightly cemented model. The second mechanism, damage, is exhibited by the q_c decrease in all three cemented models following initial liquefaction triggering. Although decreased, the q_c following cementation damage is still larger than the uncemented q_c. The final mechanism, reduced initial void ratio, is only exhibited in the heavily cemented model by the minimal change in q_c between initial liquefaction and the end of shaking. The precipitation of $CaCO_3$, approximately 2.2% by mass in the heavily cemented model, occupies void space and remains present after cemented bonds are broken. A $CaCO_3$ percentage of 2.2% decreases the actual void ratio by approximately 0.06, which implies an increase in the D_R from 38% to approximately 60% (computed using e_{max} and e_{min} for untreated sand). The minimal change in q_c observed here is consistent with work presented by Darby et al. 2017, whose previous centrifuge tests of uncemented Ottawa sand models suggest smaller q_c increases in denser models subjected to multiple shaking events as compared to loose models.

EFFECT OF CEMENTATION ON CONE PENETRATION RESISTANCE AND V_S

The effect of $CaCO_3$ content on pre-shaking mid-depth q_c and V_s is shown in Figure 8a and b, respectively. Data were obtained at 80-g at two times: before cementation (when the $CaCO_3$ content is 0%) and after cementation but before shaking (when cementation bonds are intact).

As shown in Figure 8, both q_c and V_s appear to increase linearly with increasing $CaCO_3$ content. Also shown in Figure 8 are data from Gomez et al. (2018) on MICP treated concrete sand specimens at 1-g and 10 kPa vertical effective stress. Data from the lightly and moderately cemented models fall within the range observed by Gomez et al. (2018) while data from the heavily cemented model suggests a somewhat larger increase in q_c and V_s than observed by Gomez et al. (2018) for comparable $CaCO_3$ contents.

The correlation between mid-depth q_c and V_s for uncemented and cemented models is shown in Figure 9. Penetration resistances are paired with the V_s obtained prior to each cone with the symbol shape, circles, squares, and diamonds, corresponding to cones 1, 2, and 3, respectively. Also shown in Figure 9 are data from Gomez et al. (2018) obtained at 1-g and under 10 kPa confinement on cemented samples with D_R ranging from 43-51%. The trends from both the uncemented and cemented models are reasonably consistent with the trends observed by Gomez et al. (2018), indicating an initially linear relationship below 400 m/s that becomes nonlinear as V_s increases.

LIQUEFACTION TRIGGERING AND CONSEQUENCES

Calculation of equivalent cyclic stress ratios

Irregular CSR time series are converted to equivalent uniform CSR time series using a fatigue-based cycle weighting procedure introduced by Seed et al. (1975). The relationship between CRR and the number of cycles to failure (N) is assumed to have the form:

$$CRR = a \cdot N^{-b} \quad (1)$$

Irregular cycles in an irregular CSR time series are each assigned an equivalent number of cycles using the relation:

$$N_A = \left(\frac{CSR_B}{CSR_A}\right)^{\frac{1}{b}} (1/2\ cycle) \quad (2)$$

where CSR_B is the irregular CSR cycle, CSR_A is a reference CSR, and N_A is the number of cycles of CSR_A that would cause the same damage as half a cycle of CSR_B. Equation (2) can be rearranged to calculate the uniform CSR that would cause equivalent damage in 15 cycles to the damage caused by N_A cycles of the reference CSR_A. The b-value in equations (1) and (2) is the slope of the relationship between CRR and the number of cycles to liquefaction, typically obtained by cyclic DSS or cyclic TX tests. Relatively few data have been published on the CRR versus number of cycles to liquefaction relationship for bio-cemented, clean Ottawa sand. Parra Bastidas et al. (2016) performed cyclic DSS tests and reported b-values for uncemented Ottawa sand of 0.15 and 0.17 for D_R of 40% and 80%, respectively. Ziotopoulou et al. (2018) also performed cyclic DSS tests and reported a b-value for uncemented Ottawa sand of 0.24. Darby et al. (2019) used a b-value of 0.20 to convert irregular CSRs to equivalent uniform CSRs for centrifuge tests on clean, uncemented Ottawa sand models. Burbank et al. (2013) stimulated native bacteria in reconstituted samples of Snake River sand to achieve $CaCO_3$ contents of 2.2-2.6% and 3.8-7.4%; undrained cyclic TX tests showed untreated specimens to have a b-value of 0.137, specimens with $CaCO_3$ of 2.2-2.6% to have a b-value of 0.042, and specimens with $CaCO_3$ of 3.8-7.4% to have an overall b-value of 0.07. They also observed the b-value only considering CSRs > 0.42 to be significantly larger than the b-value when only considering CSRs < 0.38, with b-values of 0.31 and 0.17, respectively. Xiao et al. (2018) performed undrained cyclic TX tests on cemented and uncemented calcareous sand samples at confining stresses of 50, 100, and 200 kPa and found uncemented samples to have a b-value of 0.195, and cemented samples to have a b-value of 0.18, with both having relatively little dependence on confining stress. A b-value of 0.20 is used in this study for the irregular CSR conversion for both

uncemented and cemented models based on Xiao et al. (2018) finding relatively small changes in b-value after cementation and the lack of published laboratory data for cemented Ottawa sand. However, the b-value is expected to decrease with increasing initial cementation level because at low amplitude cyclic loading, heavily cemented soils are expected to remain in the elastic regime, requiring a substantial increase in the number of cycles to failure. The b-value for cemented sands is hypothesized to increase after and during significant cementation degradation. It is anticipated that future studies will bring clarity to the b-value. Equivalent uniform CSRs are also reduced by 10% to account for the differences between 2-D loading in the field and 1-D loading in the centrifuge (e.g., Seed 1979).

Maximum shear strain and settlement

The maximum shear strain (γ_{max}) and incremental surface settlement during each shaking event are dependent on the level of cementation, loading, and triggering behavior. γ_{max} and incremental settlement during non-triggering and triggering events are shown in Figure 10a and c, and Figure 10b and d, respectively. At lower CSR_{15cyc}s, uncemented models tended to generate comparable or slightly larger γ_{max} than cemented models for the non-triggering events. Shear strains during non-triggering events only exceeded 0.5% in six instances: four times in the uncemented D_{R0}=53% model, once in the lightly cemented model, and once in the heavily cemented model. Shear strains during triggering events ranged from 0.2 to 1.7% in the uncemented D_{R0}=38% model with CSR_{15cyc} ranging from 0.07 to 0.1, and 0.9 to 1.6% in the uncemented D_{R0}=53% model with CSR_{15cyc} ranging from 0.1 to 0.4. Shear strains during triggering events in cemented models ranged from 0.6 to 1.7% with CSR_{15cyc} ranging from 0.2 to 0.9. Incremental settlements in non-triggering events were minimal at CSR_{15cyc} below 0.1 and ranged from negligible (0.03 mm) to 94 mm at CSR_{15cyc} ranging from 0.1 to 0.84. During

triggering events, incremental settlements ranged from negligible (0.02 mm) to 128 mm for uncemented models, and 34 to 98 mm, 40 to 80 mm, and 13 to 36 mm in lightly, moderately, and heavily cemented models, respectively. The uncemented medium dense and lightly cemented model exhibit similar behavior during triggering events with regards to both γ_{max} and incremental settlement.

Comparison to correlations

The observed liquefaction triggering behavior of the cemented models is compared in Figure 11 to existing CPT and V_s case history-based liquefaction triggering correlations for clean sands commonly used in practice. Though the comparison between centrifuge data for cemented sands and case history-based correlations for clean sands is complicated by a number of factors (discussed later), these results still provide insight into the expected behavior of bio-cemented soils subjected to cyclic loading. The shape of the symbol in Figure 11 indicates the level of cementation, with triangles, squares, and upside-down triangles corresponding to: lightly, moderately, and heavily cemented models, respectively. Shaded points indicate triggering events, open points indicate non-triggering events, and the shading intensity corresponds to the cementation level. All points correspond to mid-depth in the models and the timeline sequences are indicated by arrows. It is important to note that the centrifuge CSR_{15cyc} are for the entire loading sequence, regardless of when liquefaction is triggered, and are expected to be somewhat higher than the actual cyclic strength.

CSR_{15cyc}-q_{cN} pairs are compared to the Boulanger and Idriss (2015) CPT-based liquefaction triggering correlation for 16% probability of liquefaction (P_L) in Figure 11a. The centrifuge CSR_{15cyc}-q_{cN} pairs correspond to σ'_{v0} of 30-40 kPa, and therefore the Boulanger and Idriss (2015) correlation is plotted at a reference σ'_{v0} of 35 kPa; showing the centrifuge data at its

actual σ'_{v0} is preferable to correcting it to any other reference stress (e.g., 1 atm) because the effects of σ'_{v0} on CSR_{15cyc} and q_{cN} in cemented sands are not well defined. The q_{cN} prior to each shaking event is linearly interpolated between measured values based on incremental surface settlement. The lightly cemented model starts at q_{cN} of 44 and would be expected to trigger at a CSR_{15cyc} of about 0.09 if it was uncemented. However, the lightly cemented model does not trigger until a CSR_{15cyc} of 0.41, after which the q_{cN} only slightly decreases to a value of 40. Similarly, the moderately and heavily cemented models start at q_{cN} of 88 and 156, where they would not be expected to trigger until CSR_{15cyc} of about 0.13 and 0.37 if they were uncemented, and liquefaction was not triggered in these models until they were subjected to CSR_{15cyc} of 0.56 and 0.85, respectively, after which point the q_{cN} decreased to 60 and 94, respectively. In the moderately cemented model, q_{cN} decreased during triggering to a similar value as the lightly cemented model and exhibited similar behavior for the remainder of the shaking sequence. In the heavily cemented model, q_{cN} decreased during triggering to a similar value as the initial q_{cN} in the moderately cemented model; however, the behavior during the remainder of the shaking sequence did not follow the moderately cemented model, and the model did not trigger until once again reaching a CSR_{15cyc} of 0.84.

CSR_{15cyc}-V_s pairs are compared to the Kayen et al. (2013) V_s-based liquefaction triggering correlation for a P_L= 15% with no fines in Figure 11b. Again, the centrifuge CSR_{15cyc}-V_s pairs are plotted for their actual σ'_{v0} of 30-40 kPa because the effects of σ'_{v0} on CSR_{15cyc} and V_s in cemented sands are not well defined, and therefore the Kayen et al. (2013) correlation is also plotted at a reference σ'_{v0} of 35 kPa. The lightly cemented model starts at V_s of 209 m/s and would be not be expected to trigger at a CSR_{15cyc} below 1.7 if uncemented. The lightly cemented model triggers at a CSR_{15cyc} of 0.41, after which point the V_s decreased slightly. The moderately

and heavily cemented models start at V_s of approximately 326 and 600 m/s, and would not be expected to trigger under any level of loading. The moderately and heavily cemented models trigger at CSR_{15cyc} of 0.56 and 0.85, at which point the V_s for both models is about 300 m/s. After initial liquefaction, triggering points in the lightly and moderately cemented models tend to fall on or below the Kayen et al. (2013) correlations, whereas triggering points in the heavily cemented model uniformly fall below the Kayen et al. (2013) correlations.

The correlation between CRR_{15cyc} and q_{cN} and V_s for bio-cemented soils is complicated by the lack of data on the effects of overburden in cemented soils. Figure 12 replots the centrifuge data from Figure 11 against CPT-based (Figure 12a) and V_s-based (Figure 12b) correlations at reference σ'_{v0} of 35, 65, and 101 kPa. All triggering points and a majority of non-triggering points at all levels of cementation fall above the CPT-based triggering curves at all reference σ'_{v0} shown in Figure 12a. All triggering points in the lightly cemented model, and triggering points from later in the shaking sequence of the moderately cemented model fall between the V_s-based correlation at reference σ'_{v0} of 35 and 65 kPa in Figure 12b. Triggering points from early in the shaking sequence of the moderately and heavily cemented model tend to fall below the V_s-based correlation at reference σ'_{v0} of 101 kPa. Results in Figure 12a suggest the CPT-based liquefaction triggering correlation for bio-cemented sands would shift upward and to the left compared to uncemented sands, although some of the shift may be attributable to the undefined effects of σ'_{v0} on CSR_{15cyc} and q_{cN} in bio-cemented sands, the use of the entire loading sequence regardless of the time of triggering, the possible influence of partial drainage in the small centrifuge models, and the limited data set (e.g., one sand, one treatment type, one ground motion type). Results in Figure 12b suggest the V_s-based liquefaction triggering correlations for

bio-cemented sands would shift down and to the right compared to uncemented sands, although the same sources of uncertainty listed above also apply.

Additional research regarding the effects of σ'_{v0} and irregular loading histories (e.g., b-value, shaking history, prior liquefaction events) for bio-cemented soils are needed before CPT- and V_s- based liquefaction triggering correlations for bio-cemented sands can be confidently developed, and tests similar to those presented herein should be reproduced and expanded using a larger centrifuge. Triggering correlations require function terms to describe how q_c, V_s, and cyclic strength will vary with σ'_{v0}, but there is a lack of laboratory or field data upon which such relationships can be developed for cemented sands. For example, existing relationships for uncemented sands were generally developed using D_R as a key index parameter, whereas it is clear that D_R becomes less appropriate as an index parameter as cementation levels increase. Small centrifuge tests are subject to a number of limitations that complicate the interpretation of the results. The smaller model size limits the number of sensors that can be used, increases the effects of boundary conditions, increases the role of partial drainage during shaking, and increases the curvature of the g-field during spinning. Experience with similar studies for uncemented sands has shown that tests on the 9-m radius centrifuge produce significantly higher quality data and resolution than is possible on the 1-m radius centrifuge (Darby et al. 2016, 2019). Thus, the results of these more economical, small centrifuge model tests have demonstrated that the experimental and analytical approaches used in the present study have the potential, when extended to larger-scale experiments, to support development of liquefaction evaluation procedures for bio-cemented sands.

CONCLUSIONS

The cyclic strength of MICP cemented sand and the correlations of strength to cone penetration resistance and to shear wave velocity were evaluated with a set of centrifuge models prepared to D_{R0} of 38% and with light, moderate and heavy levels of cementation which were subjected to nine to eleven shaking events. The behavior of cemented models was evaluated against a pair of baseline uncemented models prepared to D_{R0}s of 38% and 53% and subjected to similar shaking sequences. Results indicate an increase in q_c and V_s in lightly, moderately, and heavily cemented models from 2 MPa (uncemented) to 5, 10, and 18 MPa, and from 140 m/s (uncemented) to 200, 325, and 660 m/s, respectively. Lightly, moderately, and heavily cemented models required PBAs of 0.10g, 0.17g, and 0.45g to trigger liquefaction, compared to the PBAs of 0.06g and 0.12g required to trigger liquefaction in uncemented initially loose and moderately dense models. After triggering, q_c and V_s in cemented models decreased to 5, 4, and 10 MPa and 196, 270, and 300 m/s in the lightly, moderately, and heavily cemented models, compared to minimal changes in uncemented models. After liquefaction triggering, lightly, moderately, and heavily cemented models did not subsequently trigger when subjected to the PBA required to trigger the uncemented loose model (PBA=0.06g). Maximum shear strains in cemented models ranged from 0.01 to 0.7% for non-triggering events and 0.6 to 1.7% for triggering events, with the lightly cemented model generating the largest strains. Maximum shear strains in uncemented models ranged from 0.01 to 1.04% for non-triggering events and 0.2 to 1.7% for triggering events. All cemented models required a higher CSR_{15cyc} than would be expected by existing CPT-based liquefaction triggering correlations and a lower CSR_{15cyc} than would be expected by existing V_s-based liquefaction triggering correlations. After initial triggering, the behavior of the lightly and moderately cemented models were somewhat consistent with both the CPT- and V_s-

based correlations, though the centrifuge data tended to fall above the CPT-based correlation and below the V_s-based correlation. Future research needs for development liquefaction triggering procedures for bio-cemented sands in practice were described.

ACKNOWLEDGEMENTS

Funding for this research was provided by the National Science Foundation (NSF) under NSF CA No. EEC-1449501. Operation of the centrifuge facility at the University of California, Davis was also supported by NSF as part of the Natural Hazards and Engineering Research Infrastructure (NHERI) network under award CMMI-1520581. Any opinions, findings, and conclusions or recommendations expressed in this material are solely those of the authors and do not necessarily reflect those of NSF. The authors would like the thank the staff at the UC Davis Center for Geotechnical Modeling, Charles Graddy for assistance with bacterial culturing, and Alex San Pablo for assistance with bender element fabrication and system set-up.

SUPPLEMENTAL DATA

Tables S1-S5 are available online in the ASCE Library (http://www.ascelibrary.org).

REFERENCES

Boulanger, R. W., and Idriss, I. M. (2015). "CPT-based liquefaction triggering procedure." *Journal of Geotechnical and Geoenvironmental Engineering,* ASCE, 04015065, 10.1061/(ASCE)GT.1943-5606.0001388.

Brandenberg, S. J., Wilson, D. W. and Rashid, M. M. (2010). "A weighted residual numerical differentiation algorithm applied to experimental bending moment data". *Journal of Geotechnical and Geoenvironmental Engineering.* 136(6), 854-863.

Burbank, M., Weaver, T., Lewis, R., Williams, T., Williams, B., and Crawford, R. (2013). "Geotechnical tests of sands following bioinduced calcite precipitation catalyzed by

indigenous bacteria". *Journal of Geotechnical and Geoenvironmental Engineering*, ASCE 139, 928-936.

Darby, K. M., Boulanger, R. W., and DeJong, J. T. (2017). "Effect of multiple shaking events on cone penetration resistances in saturated sand". Proceedings, 3rd International Conference on Performance-based Design in Earthquake Geotechnical Engineering (PBD-III), Vancouver, M. Taiebat et al., eds., ISSMGE Technical Committee TC203, paper 534.

Darby, K. M., Bronner, J. D., Parra Bastidas, A. M., Boulanger, R. W., and DeJong, J. T. (2016). "Effect of shaking history on cone penetration resistance and cyclic strength of saturated sand". Proceedings, Geotechnical and Structural Engineering Congress, ASCE, Phoenix, AZ, February 14-17.

Darby, K. M., Boulanger, R. W., DeJong, J. T., and Bronner, J. D. (2019). "Progressive changes in liquefaction and cone penetration resistance across multiple shaking events in centrifuge tests". *Journal of Geotechnical and Geoenvironmental Engineering*, 10.1061/(ASCE)GT.1943-5606.0001995.

Darby, K. M., Hernandez, G. L., Gomez, M. G., DeJong, J. T., Wilson, D. W., and Boulanger, R. W. (2018). "Centrifuge model testing of liquefaction mitigation via microbially induced calcite precipitation". Proc., Geotechnical Earthquake Engineering and Soil Dynamics V, Geotechnical Special Publication 290, S. J. Brandenberg and M. T. Manzari, eds., ASCE, 127-137.

DeJong, J. T., Fritzges, M. B., and Nüsslein, K. (2006). "Microbial induced cementation to control sand response to undrained shear." *Journal of Geotechnical and Geoenvirontal Engineering*, 132.11 (2006): 1381-1392.

Dobry, R., and Abdoun, T. (2017). "Recent findings on liquefaction triggering in clean and silty sands during earthquakes". *Journal of Geotechnical and Geoenvironmental Engineering*, ASCE 143(10), 04017077.

Dobry, R., Abdoun, T., Stokoe II, K. H., Moss, R. E. S., Hatton, M., and El Ganainy, H. (2015). "Liquefaction potential of recent fills versus natural sands located in high-seismicity regions using shear-wave velocity". *Journal of Geotechnical and Geoenvironmental Engineering*, ASCE, 10.1061/(ASCE)GT.1943-5606.0001239.

El-Sekelly, W., Abdoun, T., and Dobry, R. (2015). "Liquefaction resistance of a silty sand deposit subjected to preshaking followed by extensive liquefaction". *Journal of Geotechnical and Geoenvironmental Engineering*, ASCE, 10.1061/(ASCE)GT.1943-5606.0001444.

El-Sekelly, W., Dobry, R., Abdoun, T., and Steidl, J. H. (2016). "Centrifuge modeling of the effect of preshaking on the liquefaction resistance of silty sand deposits". *Journal of Geotechnical and Geoenvironmental Engineering*, ASCE, 10.1061/(ASCE)GT.1943-5606.0001430.

El-Sekelly, W., Abdoun, T., and Dobry, R. (2017). "Effect of sand overconsolidation and extensive liquefaction on K_0". Geotechnical Frontiers 2017, Geotechnical Materials, Modeling, and Testing, Geotechnical Special Publication No. 280, T. L. Brandon and R. J. Valentine, eds., 478-486.

Feng, K., and Montoya, B. M., (2017). "Quantifying level of microbial-induced cementation for cyclically loaded sand". *Journal of Geotechnical and Geoenvironmental Engineering, 143(6):06017005*

Feng, K., & Montoya, B. M. (2015). Influence of confinement and cementation level on the behavior of microbial-induced calcite precipitated sands under monotonic drained loading. *Journal of Geotechnical and Geoenvironmental Engineering*, 142(1), 04015057.

Fujita, Y., Taylor, J. L., Gresham, T. L., Delwiche, M. E., Colwell, F. S., McLing, T. L., and Smith, R. W. (2008). "Stimulation of microbial urea hydrolysis in groundwater to enhance calcite precipitation". *Environmental science & technology*, 42(8), 3025-3032.

Gomez, M. G., Anderson, C. M., Graddy, C. M. R., DeJong, J. T., Nelson, D. C., and Ginn, T. R. (2016). "Large-scale comparison of bioaugmentation and biostimulation approaches for biocementation of sands." *Journal of Geotechnical and Geoenvironmental Engineering*, ASCE, 10.1061/(ASCE)GT.1943-5606.0001640.

Gomez, M. G., DeJong, J. T., and Anderson, C. M. (2018). "Effect of bio-cementation on geophysical and cone penetration measurements in sands". *Canadian Geotechnical Journal*, https://doi.org/10.1139/cgj-2017-0253.

Kamai, R., and Boulanger, R. W. (2010). "Characterizing localization processes during liquefaction using inverse analyses of instrumentation arrays". *Meso-Scale Shear Physics in Earthquake and Landslide Mechanics,* Y. H. Hatzor, J. Sulem, and I. Vardoulakis, eds., CRC Press, 219-238.

Karol, R. H. (2003). Chemical Grouting and Soil Stabilization. Marcel Dekker, New York, NY, 558p.

Kayen, R., Moss, R. E. S., Thompson, E. M., Seed, R. B., Cetin, K. O., Der Kiureghian, A., Tanaka, Y., and Tokimatsu, K. (2013). "Shear-wave velocity-based probabilistic and deterministic assessment of seismic soil liquefaction potential". *Journal of Geotechnical and Geoenvironmental Engineering*, ASCE, 10.1061/(ASCE)GT.1943-5606.0000743.

Montoya, B., DeJong, J., and Boulanger, R. (2013). "Dynamic response of liquefiable sand improved by microbial-induced calcite precipitation". *Géotechnique*, 63(4), 302-312.

Montoya, B. M., and DeJong, J. T. (2015). "Stress-strain behavior of sands cemented by microbially induced calcite precipitation". *Journal of Geotechnical and Geoenvironmental Engineering*, ASCE, 10.1061/(ASCE)GT.1943-5606.0001302.

Okamura, M., Watanabe, S., and Nelson, F. (2017). "Liquefaction resistance of sand with pre-shaking history". Proceedings, 3rd International Conference on Performance-based Design in Earthquake Geotechnical Engineering (PBD-III), Vancouver, M. Taiebat et al., eds., ISSMGE Technical Committee TC203, paper 519.

Parra Bastidas, A. M., Boulanger, R. W., Carey, T. J., and DeJong, J. T. (2016). *Ottawa F-65 sand data from Ana Maria Parra Bastidas*. NEEShub, http://dx.doi.org/10.17603/DS2MW2R.

Raymond, A. J., Pinkse, M. A., Kendall, A., and DeJong, J. T. (2017). "Life-Cycle assessment of ground improvement alternatives for the Treasure Island, California, Redevelopment". Geotechnical Frontiers 2017, Waste Containment, Barriers, Remediation, and Sustainable Geoengineering, Geotechnical Special Publication No. 276, T. L. Brandon and R. J. Valentine, eds., 345-354.

Seed, H. B., Idriss, I. M., Makdisi, F., and Banerjee, N. (1975). *Representation of irregular stress time histories by equivalent uniform stress series in liquefaction analyses,* Report No. EERC 75-29, Earthquake Engineering Research Center, University of California at Berkeley, CA, October.

Seed, H. B. (1979). "Soil liquefaction and cyclic mobility evaluation for level ground during earthquakes". *Journal of Geotechnical Engineering Division*, ASCE 105(GT2), 201-55.

Sharp, M. K., Dobry, R., and Phillips, R. (2010). "CPT-based evaluation of liquefaction and lateral spreading in centrifuge". *Journal of Geotechnical and Geoenvironmental Engineering*, ASCE, 10.1061/(ASCE)GT.1943-5606.0000338.

Simatupang, M., and Okamura, M. (2017). “Liquefaction resistance of sand remediated with carbonate precipitation at different degrees of saturation during curing”. *Soils and Foundations, 57 (2017), 619-631.*

Stewart, D. P., Chen, Y. R., and Kutter, B. L. (1998). “Experience with the use of methylcellulose as a viscous pore fluid in centrifuge models”. *Geotechnical Testing Journal,* 21(4), 365-369.

Su, D., Ming, H. Y., and Li, X. S. (2013). “Effect of shaking strength on the seismic response of liquefiable level ground”. *Engineering Geology*, 166(2013), 262-271.

Wang, R., Hu, Q., Liu, X., and Zhang, J. (2018). “Influence of liquefaction history on liquefaction susceptibility”. Proc., Geotechnical Earthquake Engineering and Soil Dynamics V, Geotechnical Special Publication 290, S. J. Brandenberg and M. T. Manzari, eds., ASCE, 304-310.

Whiffin, V. S., van Paassen, and L. A., Harkes, M. P. (2007). “Microbial carbonate precipitation as a soil improvement technique.” Geomicrobiol. J. 25 (5), 417–423.

Xiao, P., Liu, H., Xiao, Y., Stuedlein, A. W., and Evans, M. E. (2018). “Liquefaction resistance of bio-cemented calcareous sand”. *Soil Dynamics and Earthquake Engineering, 107 9-19*

Zamani, A., and Montoya, B. M. (2017). “Shearing and hydraulic behavior on MICP treated silty sand”. Geotechnical Frontiers 2017, Seismic Performance and Liquefaction, Geotechnical Special Publication No. 281, T. L. Brandon and R. J. Valentine, eds., 290-299.

Ziotopoulou, K., Montgomery, J., Parra Bastidas, A. M., and Morales, B. (2018). “Cyclic strength of Ottawa F-65 sand: laboratory testing and constitutive model calibration”. *Proc., International Foundations Congress and Equipment Expo.* ASCE. Orlando, FL. March 6-10, 2018.

Table 1. Distribution of $CaCO_3$ content in cemented models.

	$CaCO_3$ content (% by mass)								
	Top (≈ 2 m depth)			**Middle (≈ 4 m depth)**			**Bottom (≈ 5.6 m depth)**		
Model	**A-1[1]**	**Center[1]**	**A-2[1]**	**A-1**	**Center**	**A-2**	**A-1**	**Center**	**A-2**
Lightly cemented	0.7	0.7	0.6	0.7	0.8	0.8	0.9	0.9	0.9
Moderately cemented	1.3	1.4	1.6	1.5	1.7	1.6	1.5	1.6	1.5
Heavily cemented	2.0	2.1	2.1	2.3	2.2	2.2	2.1	2.3	2.4

[1]See Figure 1 for lateral locations

FIGURE LIST

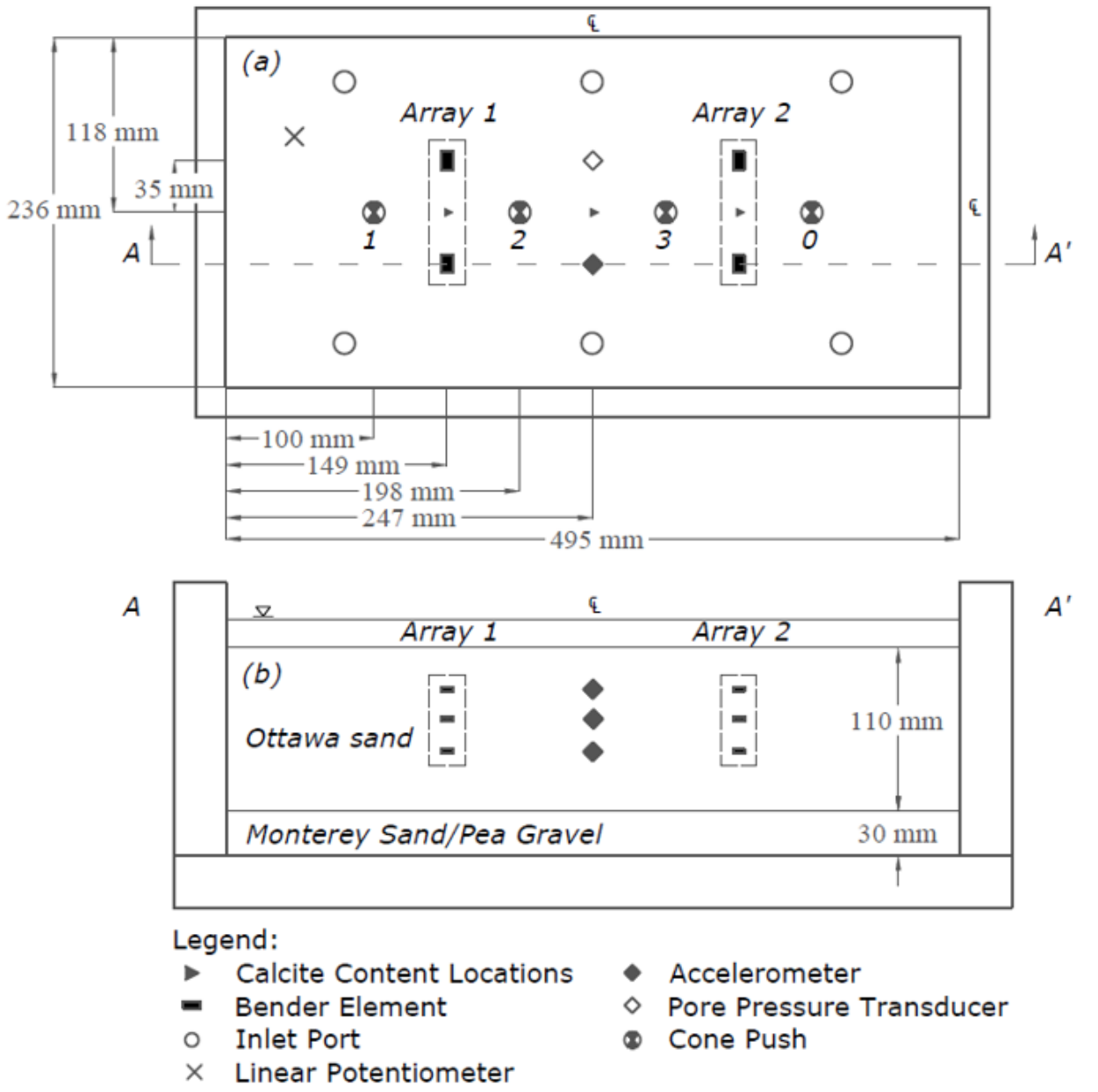

Figure 1. Representative (a) plan and (b) side view with measurement and cone locations (model units).

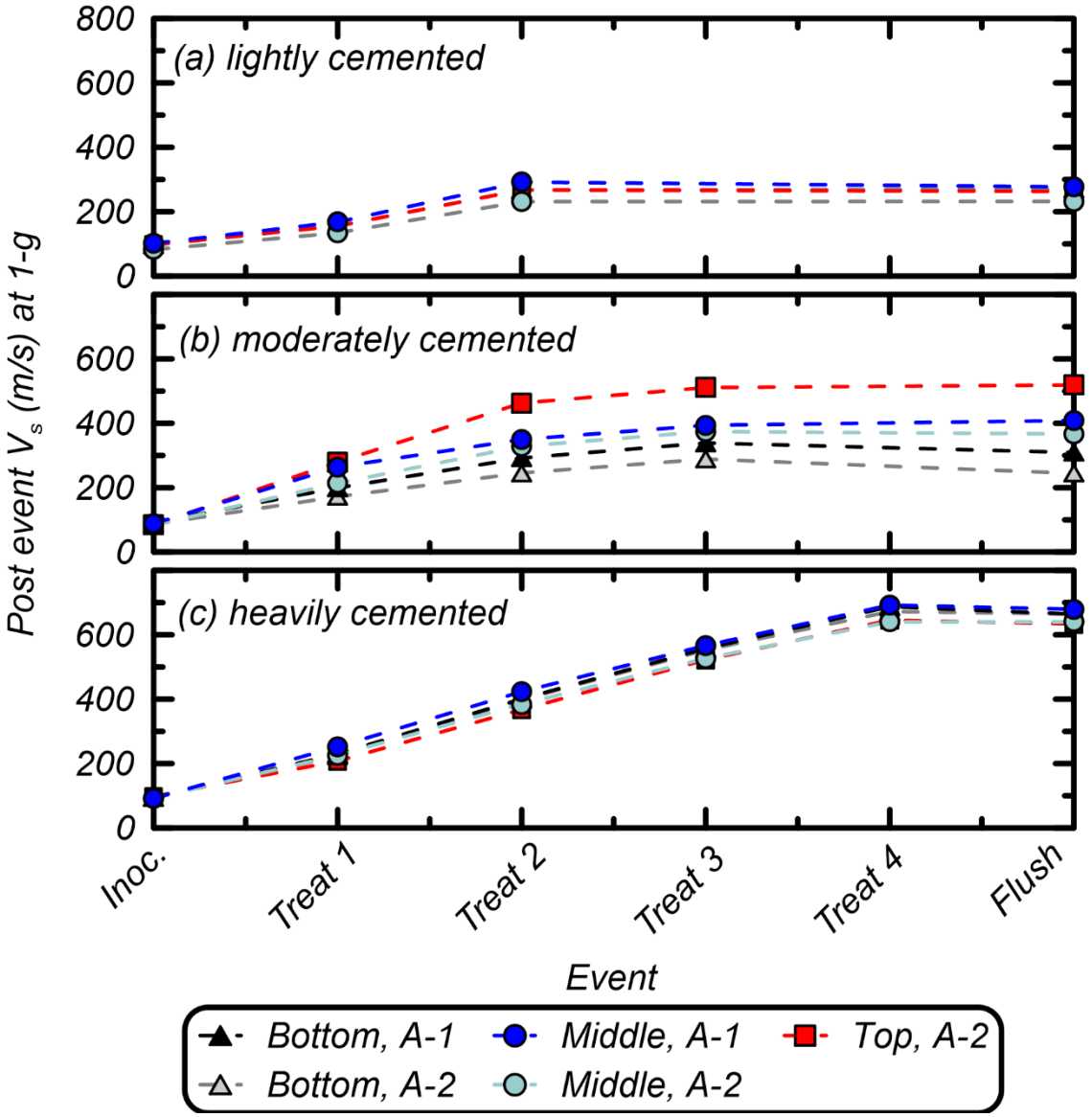

Figure 2. V_s with treatment for (a) Lightly cemented, (b) moderately cemented, and (c) heavily cemented models.

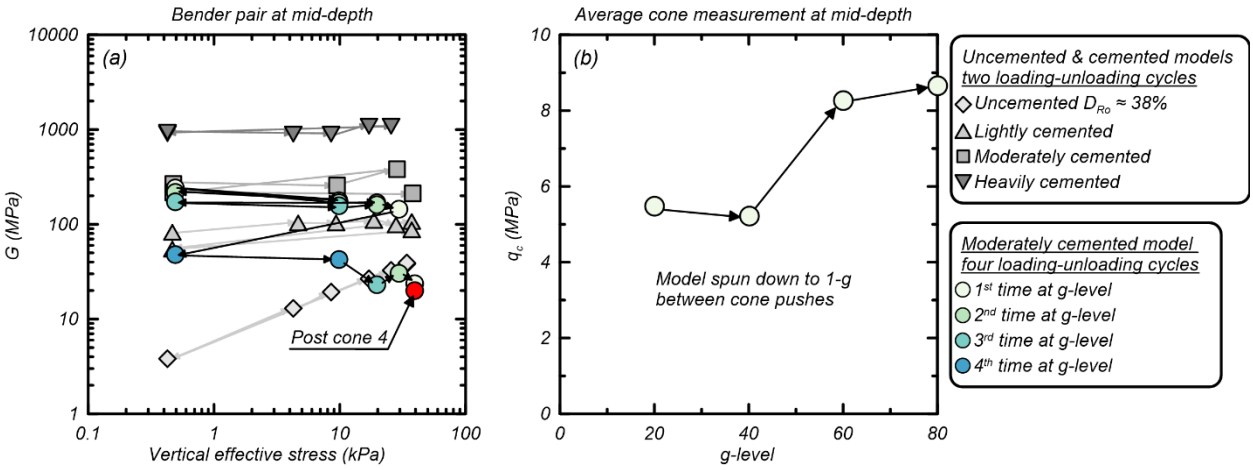

Figure 3. Progression of (a) G and (b) q_c at mid-depth with cycling of centrifuge g-level and without any dynamic shaking events.

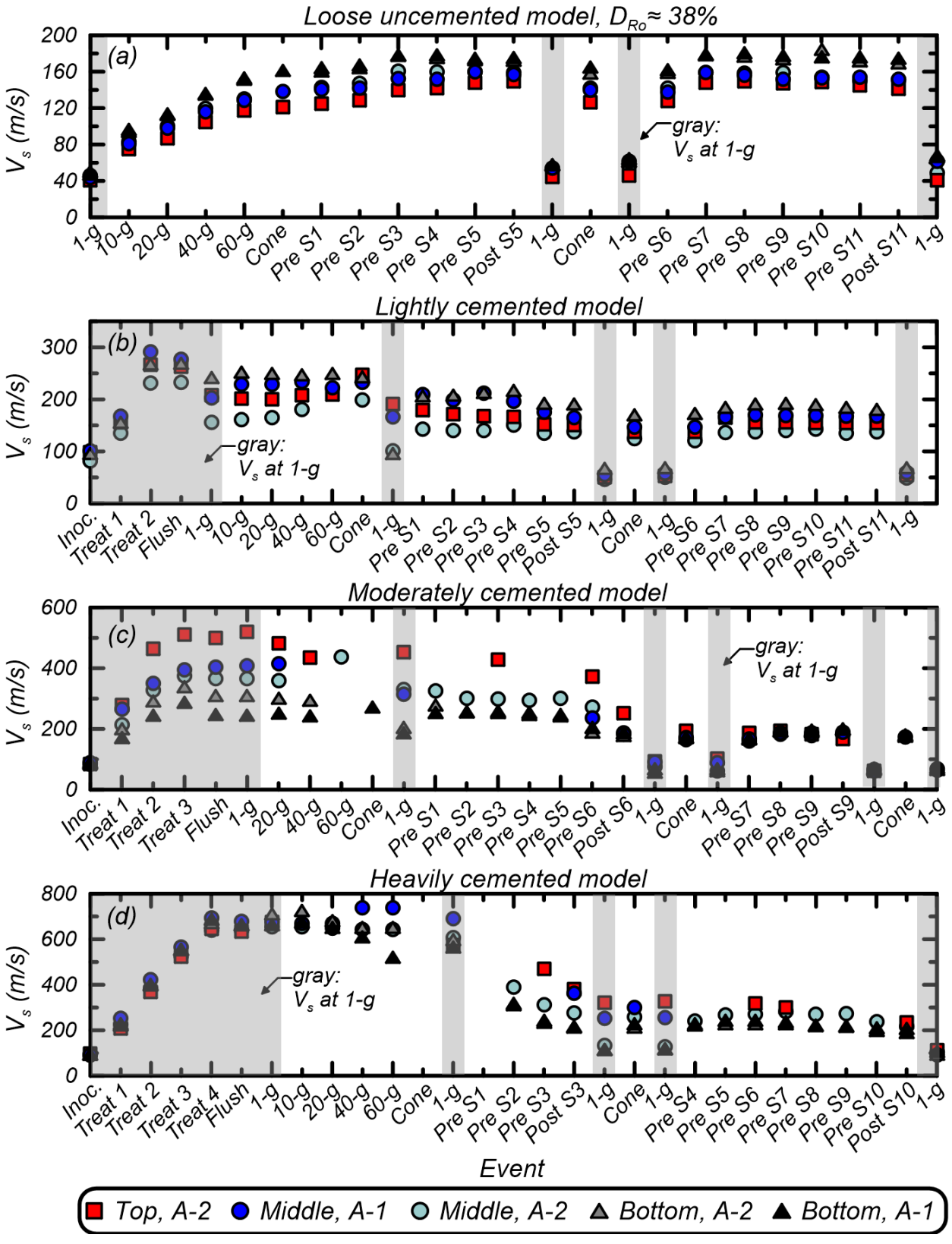

Figure 4. Progression of V_s over entire testing sequence in (a) loose uncemented, (b) lightly cemented, (c) moderately cemented, and (d) heavily cemented models.

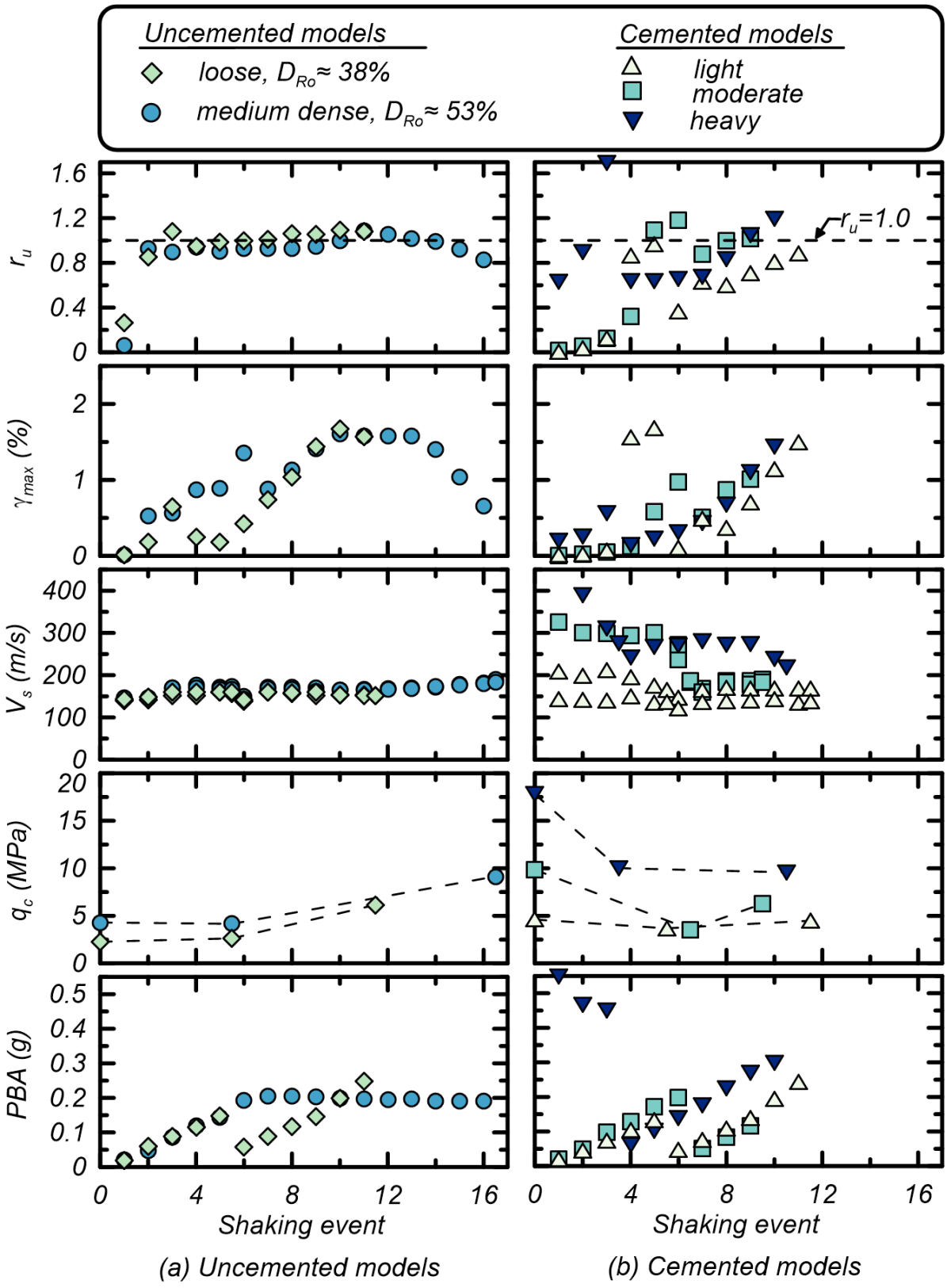

Figure 5. Shaking sequence and mid-depth responses for (a) uncemented models and (b) cemented models.

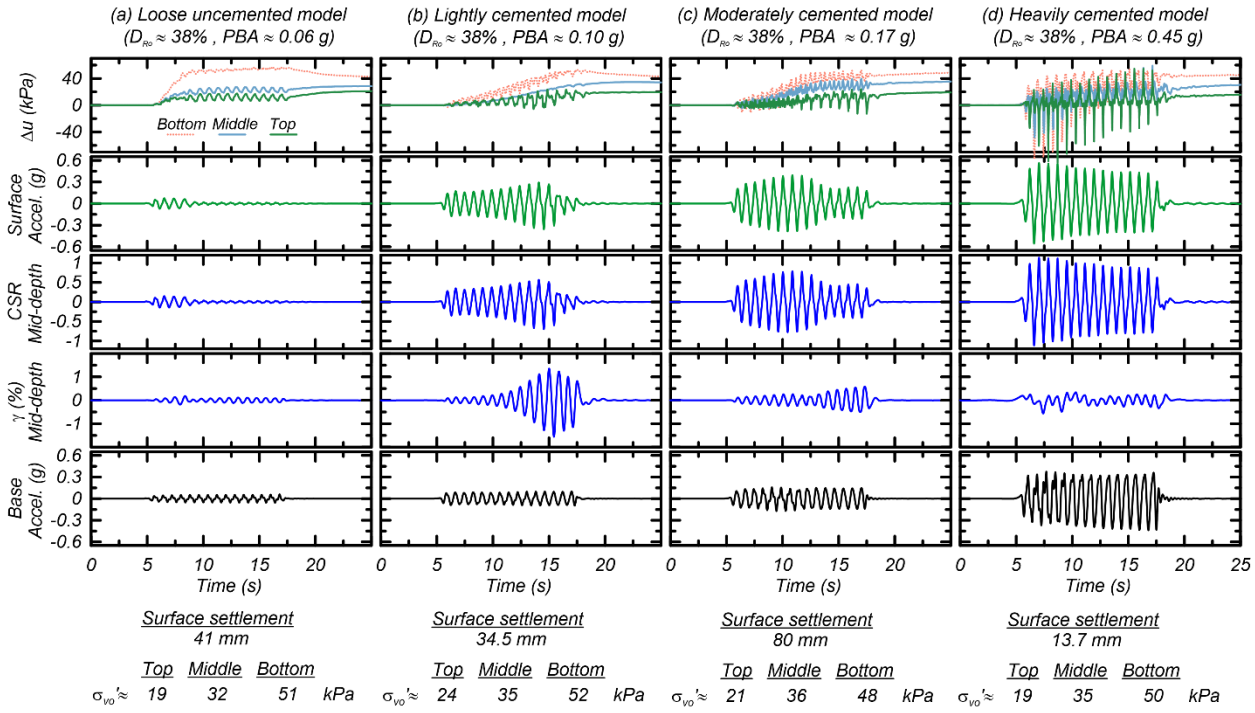

Figure 6. Comparison of dynamic responses for (a) loose uncemented, (b) lightly cemented, (c) moderately cemented, and (d) heavily cemented models during initial liquefaction triggering shaking event.

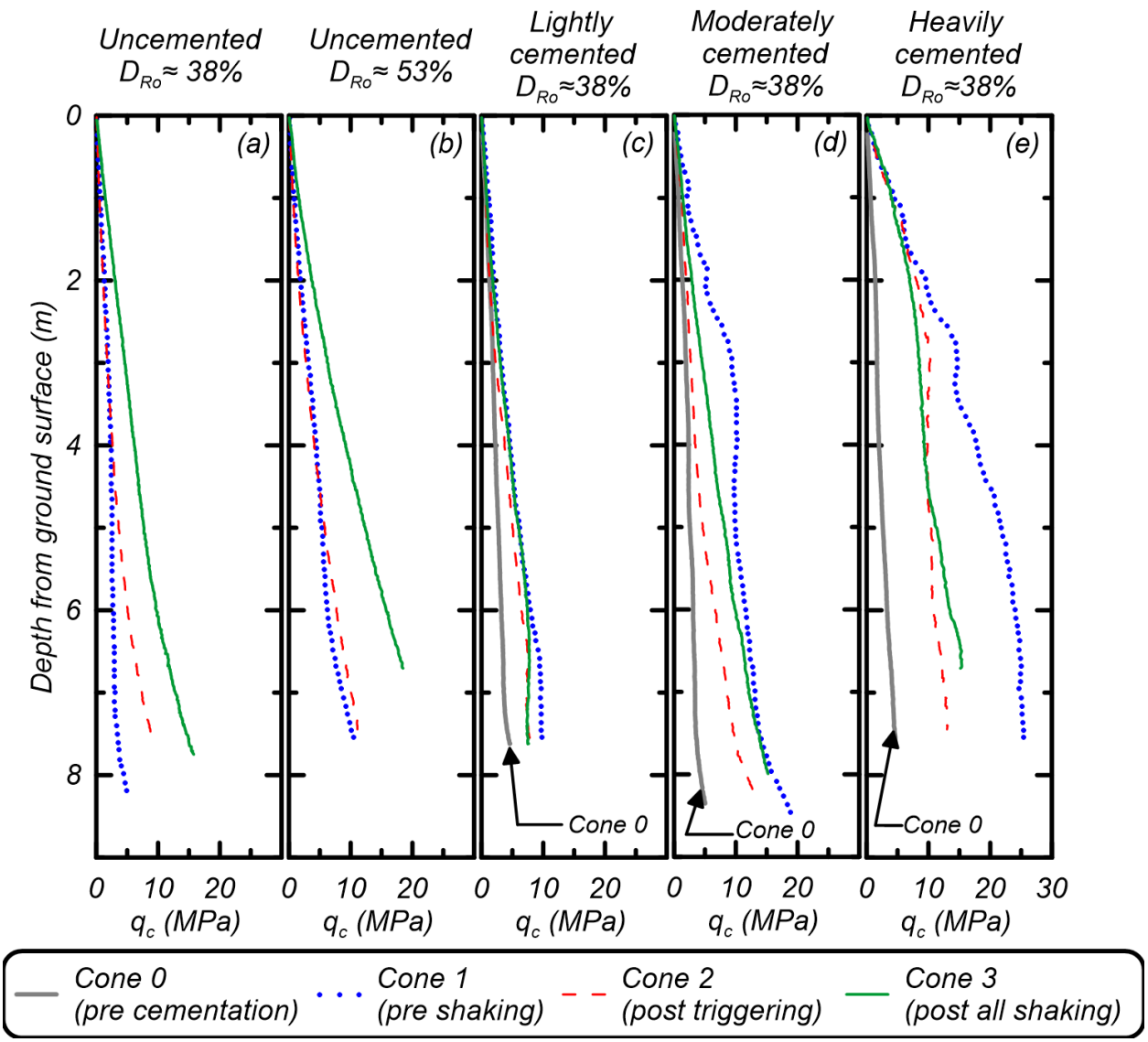

Figure 7. Progression of cone penetration resistances for (a) uncemented initially loose, (b) uncemented initially medium dense, (c) lightly cemented, (d) moderately cemented, and (e) heavily cemented models.

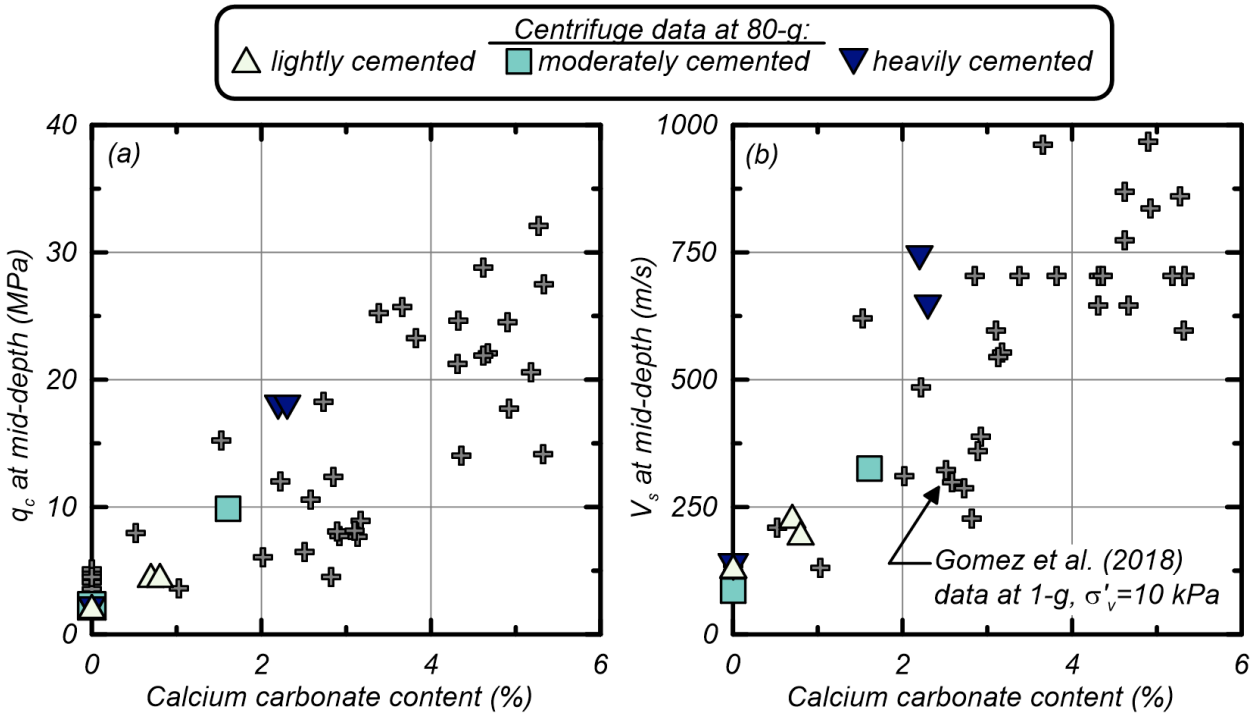

Figure 8. Effect of soil calcium carbonate content on (a) q_c and (b) V_s at mid-depth.

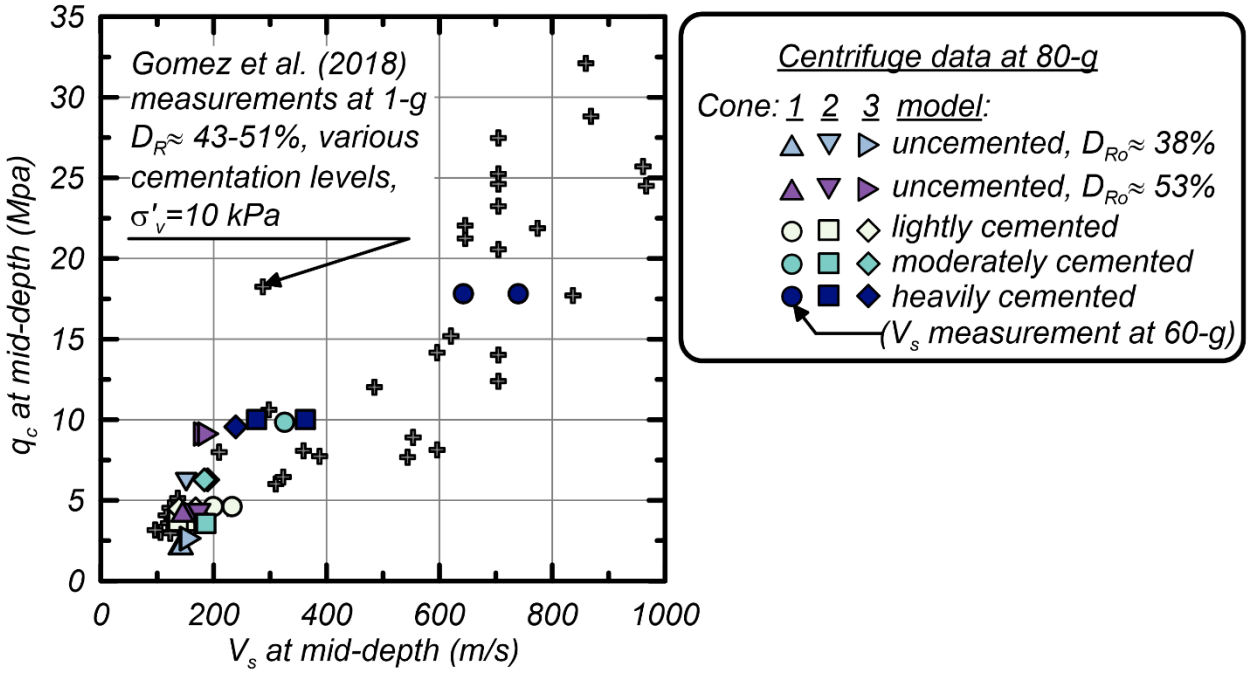

Figure 9. Effect of cementation and shaking history on q_c and V_s at mid-depth

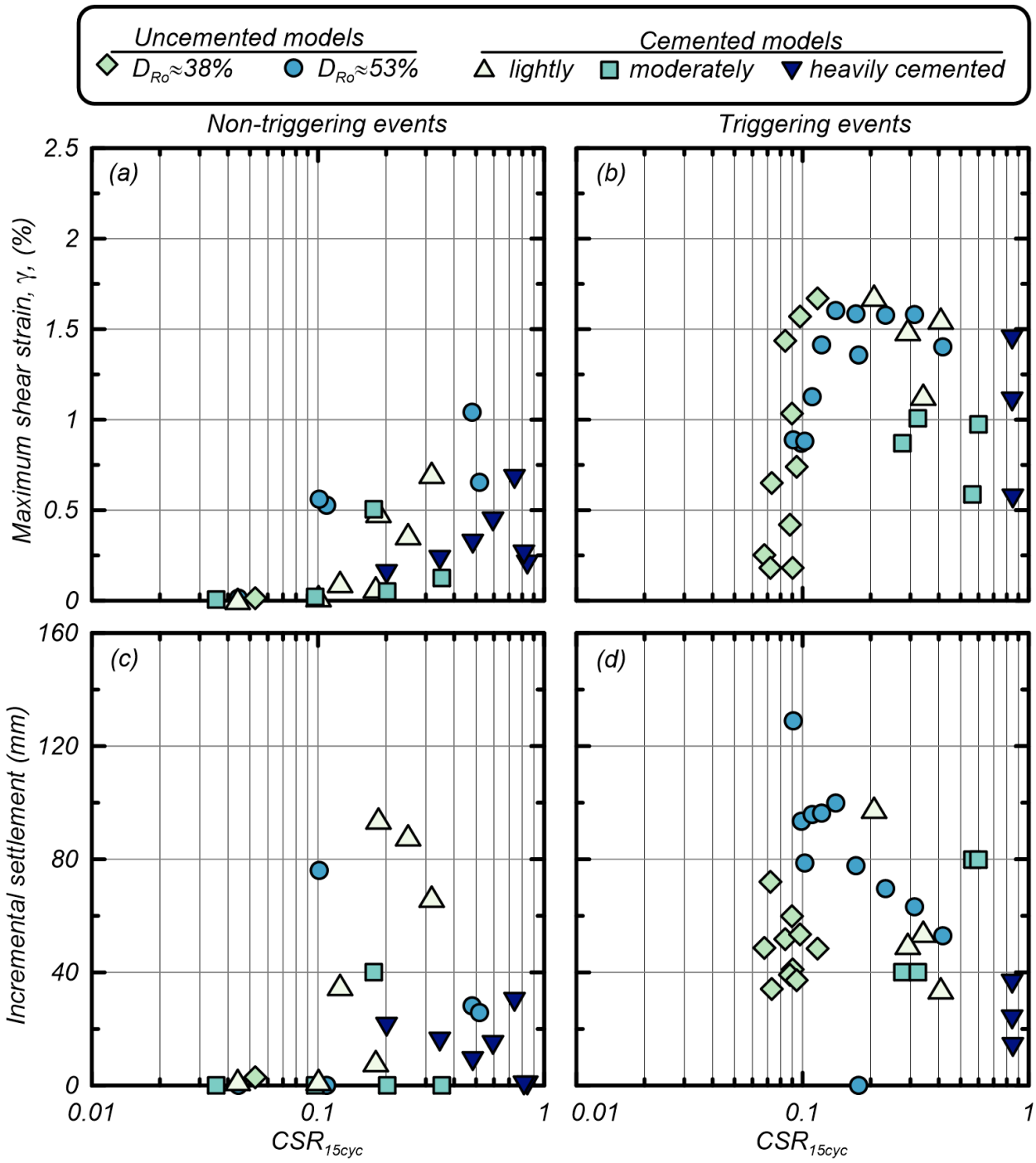

Figure 10. Maximum shear strain and CSR_{15cyc} for (a) non-triggering and (b) triggering events, and incremental settlement at CSR_{15cyc} for (c) non-triggering and (d) triggering events.

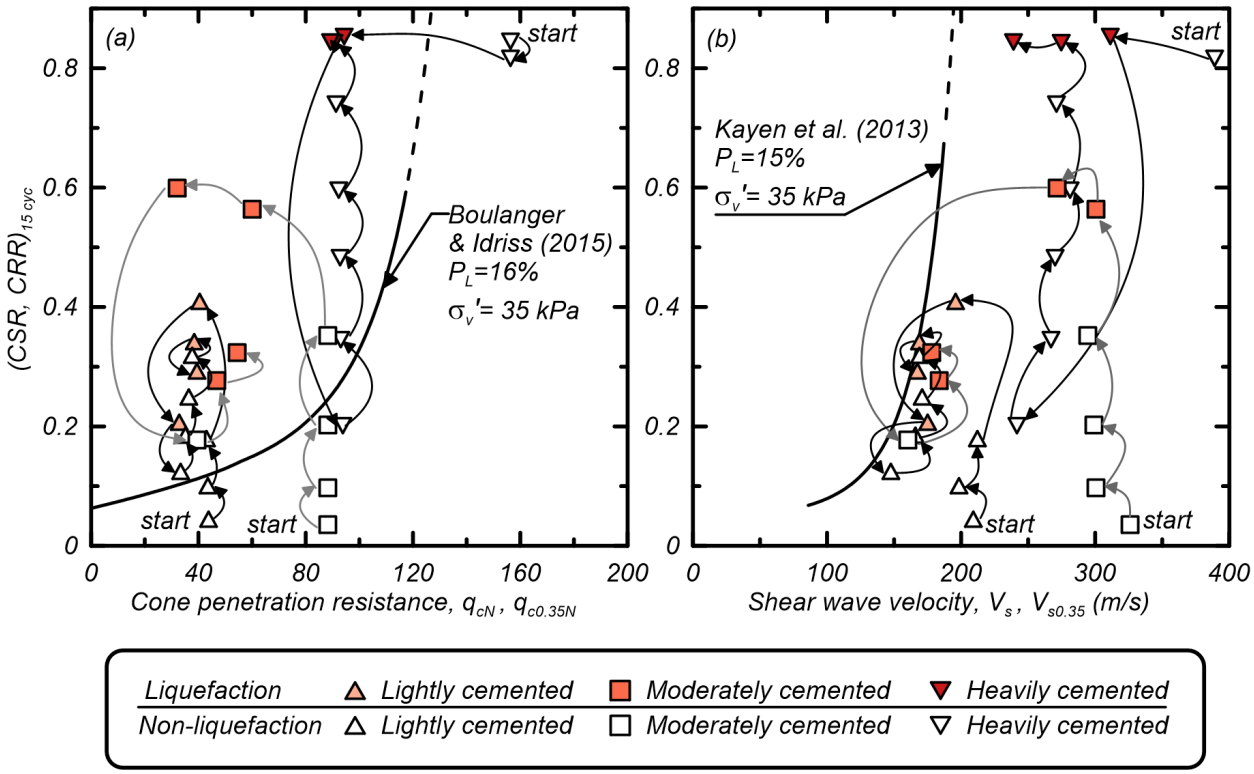

Figure 11. Comparison to existing (a) CPT-based and (b) V_s-based, liquefaction triggering correlations.

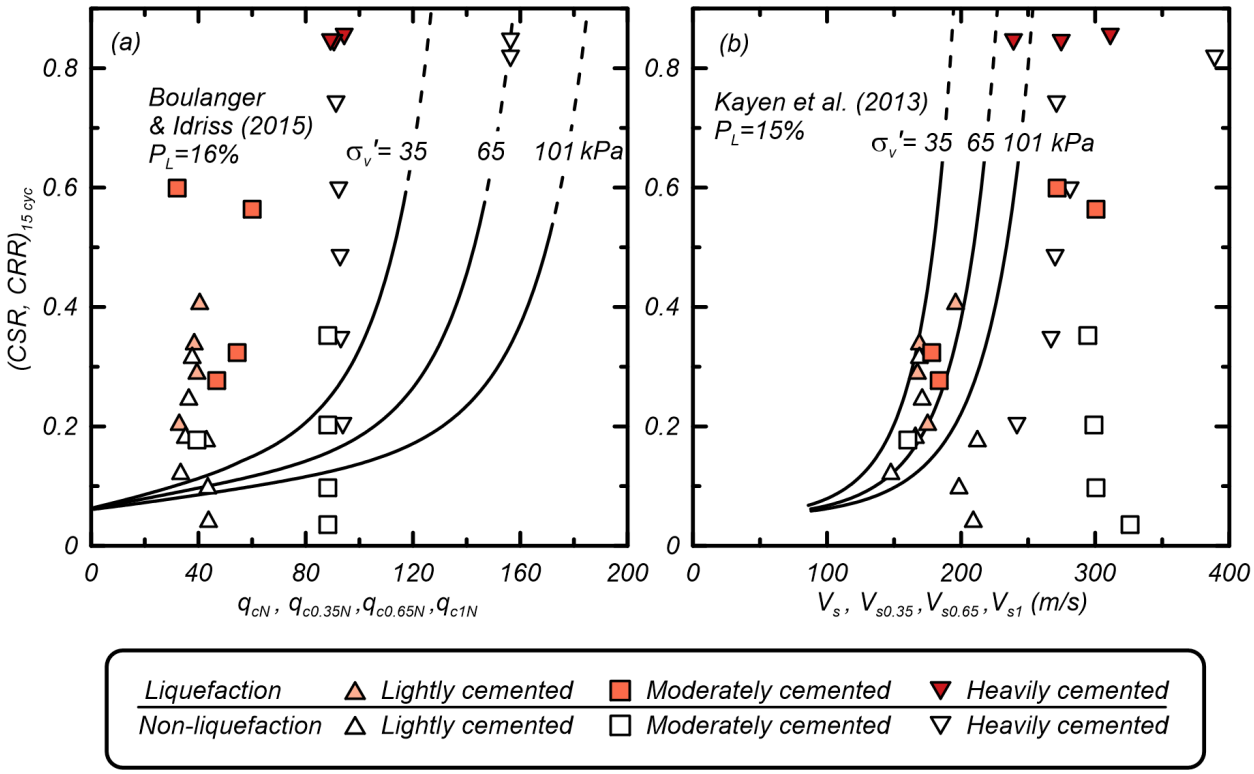

Figure 12. Effect of reference overburden stress on comparison to existing (a) CPT-based and (b) V_s-based, liquefaction triggering correlations.